Design and Evaluation of a Hybrid Passive/Active Ripple Filter with Voltage Injection

ALBERT C. CHOW

DAVID J. PERREAULT, Member, IEEE
Massachusetts Institute of Technology

Active ripple filters can substantially attenuate power converter ripple, allowing considerable reduction in passive filter component size. Investigated here is a hybrid passive/active filter topology that achieves ripple reduction by injecting a compensating voltage ripple across a series filter element. Both ripple feedforward and feedback are employed. The design of sensor, amplifier, and injector circuitry for this application is explored. The experimental results demonstrate the feasibility and high performance of the new approach, and illustrate its potential benefits. It is demonstrated that the proposed approach is most effective in cases where it is desirable to minimize the amount of capacitance in the filter.

Manuscript received September 18, 2001; revised January 13, 2003; released for publication February 27, 2003.

IEEE Log No. T-AES/39/2/812010.

Refereeing of this contribution was handled by W. M. Polivka.

This work was supported by the United States Office of Naval Research under Grants N00014-96-10524 and N00014-00-1-0381, and by the member companies of the MIT/Industry Consortium on Advanced Automotive Electrical/Electronic Components and Systems.

Authors' addresses: Massachusetts Institute of Technology, Laboratory for Electromagnetic and Electronic Systems, Room 10-015, 77 Massachusetts Ave., Cambridge, MA 02139, E-mail: (alchow@MIT.edu).

I. INTRODUCTION

Switching power converters inherently generate ripple, and typically require input and output filtration to meet ripple and electromagnetic interference (EMI) specifications. Passive LC low-pass filters have traditionally been employed to achieve the necessary degree of ripple attenuation [1]. The passive filter components often account for a large portion of converter size, weight, and cost [1–4]. Furthermore, the temperature and reliability limitations of filter capacitors can present a significant design constraint.

An alternative to the conventional passive filtering approach is to use a hybrid passive/active filter [2–10]. In this approach, a small passive filter is coupled with an active electronic circuit to attenuate the ripple. The passive filter serves to limit the ripple to a level manageable by the active circuit and to attenuate ripple components that fall beyond the bandwidth of the active circuit. The active filter circuit cancels or suppresses the low-frequency ripple components that are most difficult to attenuate with a passive low-pass filter. This approach permits a substantial reduction in the passive filter size, with potential benefits in converter size, weight, and cost.

Active filters may be characterized by whether they inject ripple voltages [3, 7] or currents [2, 4–10] to achieve ripple reduction. Controls governing the ripple correction can be derived through either feedforward [2, 9, 10] or feedback [5–8]. Feedforward controlled filters sense a ripple component and inject its inverse, while feedback controlled filters suppress ripple via high-gain feedback loop. Combinations of these mechanisms are also possible (see [3, 4] for example), and there are a wide variety of means for implementing the sensing and injection functions.

This paper focuses on a hybrid passive/active ripple filter topology that achieves ripple reduction by injecting an opposing voltage in series with the voltage ripple source. As illustrated in Fig. 1, the

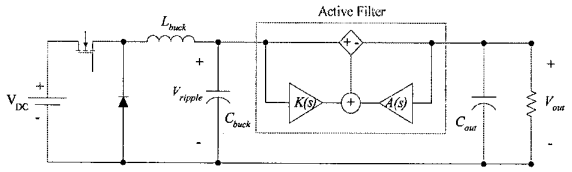

Fig. 1. Feedforward/feedback voltage ripple filter used in combination with passive filter at output of buck converter. Hybrid passive/active filter enables reduction in size of passive filter components.

active circuitry reduces the voltage ripple across C_{out} by injecting the inverse of the ripple voltage appearing across the buck capacitor C_{buck}. The injector design is challenging since it must accurately generate the desired ac injection voltage while carrying the full dc converter current. The injection signal is based on

a superposition of easily-measured feedforward and feedback voltage ripple signals. Without the feedback control, the transfer function of the feedforward path from the ripple source to the output is given by (1) for a feedforward gain of $K(s)$

$$\frac{V_{\text{out}}(s)}{V_{\text{ripple}}(s)} = 1 - K(s). \tag{1}$$

For a perfect feedforward path gain of unity, the ripple at the output would be zero. However, due to gain and phase accuracy limitations in the components, feedforward cancellation alone cannot fully attenuate the ripple. Considering the feedback path alone, the ripple source to output transfer function is

$$\frac{V_{\text{out}}(s)}{V_{\text{ripple}}(s)} = \frac{1}{1 + A(s)}. \tag{2}$$

The ripple at the output becomes small as the magnitude of gain $A(s)$ becomes large. In the feedback case, stability considerations limit the achievable feedback suppression. Combining feedforward and feedback takes best advantage of the injector circuitry and maximizes ripple attenuation. It will be shown that the proposed hybrid passive/active filter structure is attractive in cases where it is desirable to minimize the passive filter capacitance.

Section II explores the design of the proposed active ripple filter. The design of transformer-based voltage injectors, sensors, and control circuitry is addressed. A generally-applicable active damping technique is also introduced. Section III describes the application of the proposed scheme to the output filter of a buck converter, and compares the performance of the approach with that achievable with a conventional passive filter. Finally, Section IV draws conclusions and presents an evaluation of the proposed approach.

II. ACTIVE FILTER DESIGN

The active filter comprises a voltage injector circuit, a control circuit, and voltage sensors. We address each of these subsystems in turn.

A. Voltage Injector Design

The injector circuit (represented as a controlled voltage source in Fig. 1) must meet a number of challenging requirements. First, the injector must carry the full dc output current with minimal losses. Second, the injector must provide both isolation and sufficient input impedance for the active electronics. Finally, it must be able to replicate the injector signal with high fidelity. For the given constraints, a transformer proves to be an ideal choice for a voltage injection mechanism. Advantages of a transformer-based injector include minimal dc losses and inherent galvanic isolation (for coupling to control circuitry.)

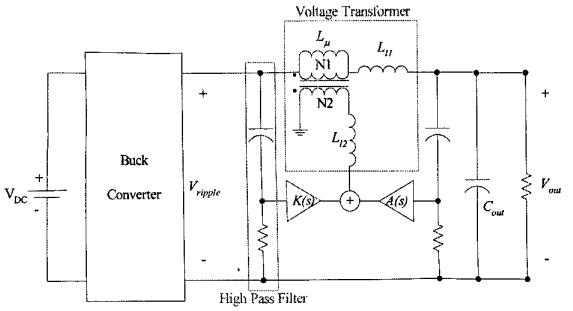

Fig. 2. Implementation of hybrid active/passive filter. Voltage sensed with an op amp via high-pass filter. Voltage injected using voltage transformer; significant transformer parasitics shown. L_μ is the magnetizing inductance. L_{l1} and L_{l2} represent leakage inductances.

A primary challenge is handling the large dc current in the system. Two different implementations that address this challenge are considered.

Fig. 2 illustrates one possible transformer-based injector, including the relevant transformer parasitics. In this case, the dc current of the converter passes through the magnetizing inductance of the transformer. This requires that the core be properly sized and gapped to prevent saturation under this heavy bias condition. The transformer magnetizing inductance L_μ and turns ratio must also be selected such that the transformer presents sufficient impedance so that the signal-level amplifier is not loaded. The amplifier circuitry is required to generate an ac voltage of magnitude:

$$V_{\text{circuit}} \approx \frac{N_2}{N_1}|V_{\text{ripple}}| \tag{3}$$

and a current of magnitude:

$$I_{\text{circuit}} \approx \frac{N_1}{N_2}\frac{|V_{\text{ripple}}|}{\omega_{\text{ripple}} L_\mu} \tag{4}$$

where L_μ is the magnetizing inductance measured on the transformer's primary side, $|V_{\text{ripple}}|$ is the magnitude of the ripple to be cancelled, and ω_{ripple} is the fundamental frequency of the ripple. The magnetizing inductance (and hence transfomer core size) is determined by the output current and dissipation limits of the amplifer circuitry. The transformer turns ratio is used to match the voltage and current drive levels of the amplifier to those required for voltage ripple cancellation. To maximize amplifier use and minimize injector size, the turns ratio should be selected to fully utilize the available amplifier voltage and current swing. For example, the amplifier in the prototype system has an output voltage limit of $+/-6$ V, and a current limit of $+/-$ 100 mA. To suppress a 2.5 V peak-to-peak ripple voltage, a turns ratio of 1 : 5 is selected. Given a 125 kHz fundamental ripple frequency a magnetizing inductance of 5 μH is selected so that the current drive capability of the amplifier is not exceeded.

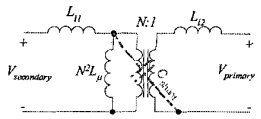

Fig. 3. Transformer model including parasitics. Parasitics can cause magnitude and phase errors. Transformer used in prototype has turns ratio of 5 : 1.

Nonidealities in the transformer affect the controls of the filter and therefore play an important part in the design. The use of feedforward ripple cancellation requires that the ripple be both sensed and injected with great accuracy. Therefore, the injector must have negligible magnitude attenuation and phase shift for the frequency range of interest; any phase or magnitude error will greatly degrade the performance of the feedforward control. For an ideal transformer, the voltage appearing on the primary side is a perfectly scaled version of the voltage on the secondary side. However, transformer parasitics [11, 12] (illustrated in Fig. 3) can limit the injector performance. Experimental results have verified that the primary to secondary shunt capacitance C_{shunt} does not affect the behavior of the injector for the frequency range of interest, and is therefore neglected. However, the secondary side leakage inductance L_{l2} forms a voltage divider with the secondary side magnetizing inductance, resulting in a magnitude error. A winding geometry that minimizes leakage inductance is advantageous. After investigating several geometries, while keeping implementation ease in mind, an interleaved primary over secondary winding method was selected for the prototype, as this resulted in a low value of L_{l2}.

Stability is a major concern when employing feedback-based control, and is the major factor limiting achievable attenuation. The injector transformer is in the feedback loop, so any phase lag added by the transformer can greatly decrease stability. An ideal transformer adds zero phase lag, but the parasitic inductance on the primary side L_{l1} plays a surprisingly important role in the stability of the system. As described in Section II, L_{l1} and the output capacitor C_{out} form a second-order low-pass filter, and the phase shift associated with this parasitic filter can affect the stability of the feedback control. As a result, the transformer design should minimize L_{l1} to ease the constraints on the control design.

It is advantages for both feedforward and feedback control to minimize the leakage inductances, which depends on two factors: winding geometry (as mentioned above) and core gap length. Reducing gap size reduces the leakage inductance, but it substantially increases transformer size. The main factors that determine transformer size are magnetizing inductance L_μ, maximum allowable flux density B_{max}, gap size, maximum current $I_{\mu,\text{max}}$, and winding space, which are highly constrained by the

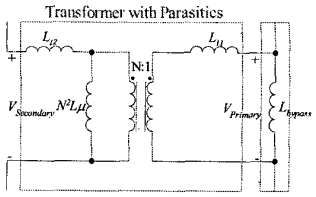

Fig. 4. Injector implementation that uses bypass inductor in parallel with high-frequency transformer. Significant transformer parasitics L_μ, L_{l1} and L_{l2} are also represented. High-frequency transformer has turns ratio of 5 : 1.

particular application. For instance, the maximum magnetizing (bias) current is determined by the converter current rating. The magnetizing inductance value is set by the active circuitry constraints of (3) and (4). The saturation flux density of the core material B_{sat} and ac losses determine the maximum allowable flux density B_{max}. For a given current, magnetizing inductance, and maximum allowable flux density, there is a direct relationship between A_L (inductance factor nH/turns^2) and core area A_{core}:

$$A_{\text{core}} = \frac{I_{\mu,\text{max}}\sqrt{L_\mu A_L}}{B_{\text{max}}} \tag{5}$$

where A_L is inversely proportional to the gap length, which typically correlates with leakage inductance.[1] Thus, there is a tradeoff between the leakage inductance and the core size. For instance, the prototype injector could be implemented using an RM14 core with a relatively small gap. To reduce core size, the prototype injector is built on an RM12 core because it is the smallest core with adequate space for both windings. This results in a primary side leakage (L_{l1}) of 0.156 μH (3.4%). The secondary side leakage (L_{l2}) is 2.3 μH (2.5%). The corresponding gain of 0.98 is calculated from (6)

$$\text{Gain} = \frac{N^2L_u}{L_{l1} + N^2L_u} = \frac{V_{\text{out}}}{V_{\text{in}}}. \tag{6}$$

To the extent that this gain is known and repeatable, it can be compensated for in the control design.

B. Alternative Voltage Injector

An alternative method for implementing the injector is to use a bypass inductor in parallel with a high-frequency transformer, as illustrated in Fig. 4. In this approach, the bypass inductor, which is implemented with a gapped core and wound

[1]Such a relationship is expected based on a simple magnetic circuit model. Leakage path reluctance appears in parallel with the reluctance of the gapped branch of the magnetic path, and both are in series with the driving MMF and the remaining core reluctance. As the gapped-path reluctance increases, more flux is driven through the leakage path (both absolutely and in percentage terms) resulting in both absolute and percentage increases in leakage inductance.

with large-gauge wire, serves as the dc bypass element. This function is accomplished by the magnetizing inductance L_μ in the previous case. The high-frequency transformer is implemented with a much smaller ungapped core using small-gauge wire. This element serves as the means for voltage injection. The relative winding resistances determine the dc current sharing between the inductor and the transformer, while the ac characteristics are determined by the relative inductances. The high-frequency transformer must be implemented with a nongapped core to keep leakage inductances comparable to the single-core implementation. The gain of the voltage injected with this approach may be calculated as

$$\text{Gain} = \frac{N^2 L_u}{N^2 L_u + L_{l2}} \left(\frac{L_{\text{DC}}}{L_{l1} + L_{\text{DC}}} \right) = \frac{V_{\text{out}}}{V_{\text{in}}} \tag{7}$$

By minimizing the leakage inductances L_{l1} and L_{l2} the gain is maximized. It should be noted that in the previous implementation, only L_{l2} caused a magnitude error in the injected signal. In the two-core approach L_{l1} also causes a magnitude error, because it forms a voltage divider with the bypass inductor. This approach can thus lead to a larger magnitude error.

A prototype ac transformer was wound on a nongapped RM5 core, while the bypass inductor was wound on a gapped RM10 core. The combined volume of the inductor and transformer is 4884 mm^3. The single-core design has a volume of 8340 mm^3. The two component approach thus yields almost a 50% reduction in total volume. The ac transformer magnetizing inductance L_μ is 50 μH, L_{l1} leakage is 0.148 μH (or 0.4%) and the L_{l2} leakage inductance is 1.32 μH (or 0.15%). This is much lower than in the previous design. However, the gain is decreased, 0.92 as compared with 0.98 yielded by the single core design. The example confirms a volume verses gain tradeoff with the two magnetic component implementation in comparison with the single magnetic component implementation.

C. Active Circuitry Design

The design of the active circuit is greatly dependent upon the switching frequency of the dc/dc converter. The example power converter considered here has a fundamental switching frequency of 125 kHz. Therefore, to attenuate the fundamental and several of its harmonics the passband should include 100 kHz and beyond.

The active circuitry, illustrated in Fig. 5, comprises a feedback amplifier, a feedforward amplifier that also acts as a summing amplifier for the feedback signal, and a power gain stage. The feedforward controller must be implemented with exact gain, minimal phase shift, and low distortion. The desired gain of the feedforward path is equal to the turns ratio divided

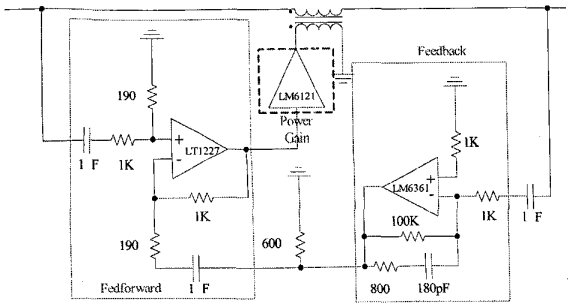

Fig. 5. Three-stage amplifier implementation of control. From top to bottom and left to right: first stage provides the power gain to drive the injector transformer, second stage serves as the feedforward gain and the summing point for the feedback control, last stage is the feedback gain with minor-loop compensation.

by the gain (less than 1) caused by the transformer parasitics:

$$\text{Gain}_{\text{single}} = \frac{N^2 L_u + L_{l1}}{N L_u} \tag{8}$$

$$\text{Gain}_{\text{two}} = \frac{N^2 L_u + L_{l2}}{N L_u} \left(\frac{L_{l1} + L_{\text{DC}}}{L_{\text{DC}}} \right). \tag{9}$$

This way, the feedforward gain can be used to compensate the magnitude error due to transformer gain (less than 1). The single-core injector transformer requires a feedforward gain of 5, while the two-component injector requires a gain of 5.2, since its transformer gain (less than 1) is smaller. It is important to note that manufacturing variations can make this gain compensation challenging, particularly for the two-component implementation.

The prototype amplifier design uses readily available discrete components. A current feedback op-amp, LM1227, is used for the feedforward gain because it achieves the necessary gain, bandwidth, and slew-rate requirements for this application. The feedforward op amp also acts as a summer, which allows this stage to incorporate the feedback control signal. A high-speed buffer, LM6121, is used to implement the power gain stage. It is able to provide +/ − 100 mA of current with +/ − 6 V output swing at a bandwidth of 50 mHz. A high-frequency voltage-feedback op amp, LM6361, is used for the feedback amplifier instead of a current feedback op amp because it simplifies the feedback control design. The LM6361 has a predictable gain and phase shift.

There are two main limitations that dominate the feedforward system: nonexact gain compensation and non-zero amplifier output resistance. Due to parameter variations of the inductor and transformer, the feedforward gain cannot completely compensate for the magnitude error. Assuming zero phase error, the percentage error in magnitude corresponds directly to the percentage of residual ripple. For example, a 10% magnitude error results in a 10% residual ripple. The non-zero output impedance of the power gain

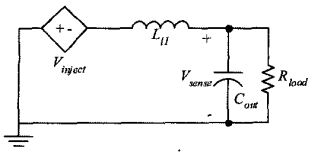

Fig. 6. Circuit represention of the voltage injector loaded with the output capacitor. Voltage source represents injected signal on voltage transformer. To simplify analysis the buck capacitor and damping due to R_{load} has been neglected. Feedback signal is sensed across the output capacitance.

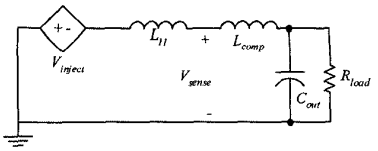

Fig. 7. Circuit represention of voltage injector loaded with output capacitor and series compensating inductor. Voltage source represents injected voltage. To simplify analysis, buck capacitor and damping due to R_{load} has been neglected. Feedback signal is sensed between the two inductors.

stage causes a phase error, because it forms a high pass filter with the magnetizing inductance on the secondary side of the transformer:

$$\frac{V_{\text{transformer}}}{V_{\text{circuit}}} = \frac{sN^2L_u}{R_{\text{out}} + sN^2L_u}. \tag{10}$$

For perfect gain, the percent residual ripple depends on the phase error ϕ in the following manner:

$$\text{Percent\_}V_{\text{residual}} = \sqrt{(1-\cos\phi)^2 + \sin^2\phi} * 100. \tag{11}$$

The pole associated with the output resistance is at 6.4 kHz in the prototype. Although it is well below the fundamental frequency, there is a slight phase shift of 3 deg at the switching frequency. This results in a maximum 95% ripple cancellation by the feedforward system, as per (11). The corresponding magnitude error is negligible, given knowledge of the transformer parasitics. Therefore it is these errors in magnitude and phase that prevent perfect ripple nulling.

The design of the feedback controller is not only dependent on switching frequency, but also on the stability of the control loop. The effectiveness of feedback control is directly dependent upon gain. Thus maximizing gain, without instability, is most desirable. Assuming C_{buck} is much greater than C_{out}, the leakage inductance L_{l1} and the output capacitor C_{out} form a low-pass filter, illustrated in Fig. 6. This two-pole filter causes an additional -180 deg phase shift from V_{inject} to V_{sense}. Neglecting damping and assuming that the buck capacitor is nearly ac ground, the following equation gives the transfer function from the injected voltage to sensed voltage:

$$H_{\text{injector}}(s) = \frac{V_{\text{sense}}(s)}{V_{\text{inject}}(s)} = \frac{-1}{1 + (L_{l1}C_{\text{out}})s^2}. \tag{12}$$

The higher the unity-gain crossover frequency, the larger the attenuation will be across the frequency range of interest. However, if the -180 deg phase shift occurs before the unity-gain crossover, then the system will be unstable. The parasitic low-pass filter in the prototype occurs around 1.5 mHz, therefore it restricts the gain across the frequencies of interest, in this case from 125 kHz to 1 mHz.

To overcome this limitation, a small inductive element L_{comp} is added between the sense point and the load; see Fig. 7. In the prototype system this was implemented as a small magnetic bead. This results in the addition of two zeros after the two poles:

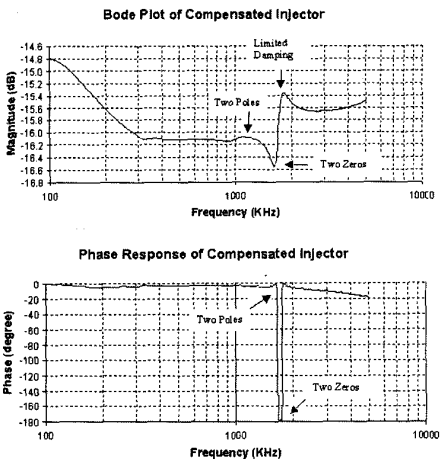

Fig. 8. Transfer function from injected to sensed voltage. Two poles are due to low-pass filter formed by $L_{l1} + L_{\text{comp}}$ and C_{out} adds a $-180°$ phase shift. L_{comp} adds the two zeros and C_{out} brings phase back to 0°. Magnitude shows peaking near poles and zeros of system, which is due to limited damping.

$$H_{\text{comp\_inj}}(s) = \frac{V_{\text{sense}}(s)}{V_{\text{inject}}(s)} = \frac{-(L_{\text{comp}}C_{\text{out}})s^2 - 1}{s^2(L_{\text{comp}} + L_{l1})C_{\text{out}} + 1}. \tag{13}$$

If L_{comp} is much smaller than L_{l1} then the zeros occur just after the poles. Therefore the phase of the system approaches -180 deg (never reaching it due to damping) and then returns to zero degrees. Fig. 8 shows the frequency response of $H_{\text{comp\_inj}}(s)$ for the prototype system.

The attenuation of the ripple will be greatly degraded at the frequency where the minimum of magnitude response occurs. Furthermore, the ripple at this frequency is greater with feedback filtering than without. This is because not only is the magnitude at a minimum but the phase is nearly -180 deg, which makes the gain $A(s)$ a negative number less than one, thus causing the attenuation to become less than one. These poorly damped pole and zero pairs make the design of the feedback control loop difficult.

One solution is to add additional series or shunt damping. In either case, resistive damping needs to be added on the load side of V_{sense} of Fig 7, thereby allowing a damping term for both the zero and the pole. A shunt damping leg is chosen for this particular application because it can be easily and inexpensively implemented with a capacitor and resistor. A series damping topology would require an inductor in parallel with a resistor. The inductor would be required to withstand the large bias current, thus making it large. This problem is similar to the one facing the design of the transformer. As discussed in the following section, both damping schemes can also be implemented with a simple active circuit.

With compensation and damping, the gain can be increased: the unity gain crossover frequency extends past 1.5 mHz. The small ferrite bead (bead number 2673021801) used as the compensation inductance in the prototype not only adds inductance but extra resistive damping. This allows the unity-gain frequency to occur at 10 mHz. Minor loop compensation is used to further increase stability. The gain of the prototype system is 50 at 125 kHz and decreases 20 dB per decade. Since the gain is not infinite, the feedback controller is not able to completely eliminate the ripple.

D. Active Damping

The passive components used for series and shunt damping schemes can be larger than the filter elements themselves. For instance, the capacitor of a damping leg is usually an order of magnitude larger than the value of the output capacitor [1]. This is also true for the series damping topology. Active damping techniques are an attractive approach for reducing passive component size. A series damping element can be implemented with a transformer in conjunction with a gain stage [13]. Since the damping element must lie outside of the feedback loop, the injection transformer cannot be reused for this purpose. Hence, the series damping topology was not chosen due to its complexity and its need to place an additional transformer in the dc power path. A shunt damping circuit, consisting of a capacitor in series with a resistor, is chosen for its implementation ease.

An active shunt damping scheme requires a topology where the capacitor is enhanced. Just as with active ripple filters, this can be accomplished in a variety of topologies: current sense/current drive, voltage sense/current drive, current sense/voltage drive, and voltage sense/voltage drive. Here we introduce the current sense current drive active damping circuit illustrated in Fig. 9(b). The current that flows into the transistor base through the capacitor C_{small} is amplified by a current gain β. The small-signal model of the transistor input resistance r_π is in series with the capacitor C_{small} in Fig. 9(c). The

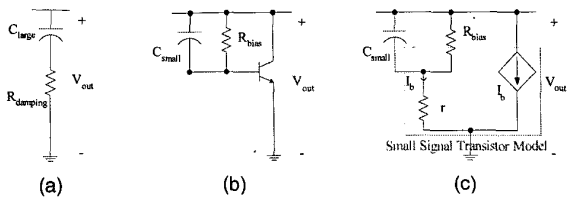

Fig. 9. (a) Conventional passive shunt damping circuit. (b) Proposed active damping circuit. (c) Small-signal model of active damping circuit. Transistor allows C_{small} to replace C_{large}, since current that flows through C_{small} is magnified by the beta of the transistor. Input resistance r_Π of transistor serves as damping resistor.

effective shunt impedance thus becomes

$$Z_{equivalent} = \frac{r_\pi + \dfrac{1}{sC_{small}}}{\beta + 1}. \tag{14}$$

The overall impedance is reduced by $\beta + 1$. In other words the capacitance in increased by $\beta + 1$, thus $C_{eq} = (\beta + 1)C_{small}$ and $R_{eq} = r_\pi/(\beta + 1)$.

The proposed active damping implementation employs only a single transistor. Since damping is required for only lower frequencies, a low-end transistor (i.e. $f_T \sim 300$ mHz, $B \sim 100$) will suffice. The effective damping resistance is approximately $1/g_m = V_t/I_c$. Therefore this sets the bias current requirement I_c of the transistor, and the dissipation. Simulations have demonstrated that the 0.6 ohms is the largest resistance acceptable for a fair amount of damping, which require about 45 mA of bias current. This particular implementation uses a 2N2219 transistor with a beta of about 100. A 50 kΩ resistor is employed to bias the transistor into the linear region; a 1 nF capacitor is used as the amplified capacitance. It should be noted that the aforementioned circuit is limited in its robustness, due to basis stability and gain. Nevertheless, there are many circuit topology variations that are able to correct for these limitations (e.g., the use of a current-regulating diode in place of a resistor for bias stability). Overall, the active damping circuit replaces a comparable passive damping leg requiring a 0.22 Ω resistor and a 1 μF capacitor.

Test results show that the active damping leg performs comparably to the passive damping leg around the corner frequency of the LC filter (see Fig 10). The passive damping leg is implemented with a 1 μF capacitor and a 0.22 Ω resistor. The resistor is used in combination with the equivalent series resistance (ESR) of the capacitor to form the needed 0.6 Ω of damping. For frequencies below the knee, less than 200 kHz, the active damping leg has larger impedance than the passive damping leg. This is also true of frequencies greater than the corner frequency, above 3 mHz. The performance of the active damping leg for frequencies above and

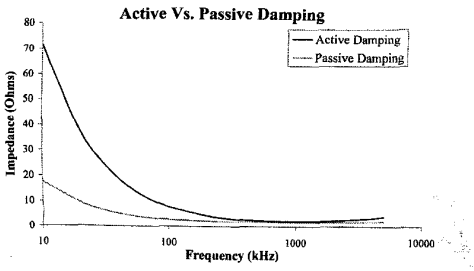

Fig. 10. Shows comparison of impedances between active and passive damping topologies. Performance of damping leg is only affected by its behavior at frequency of interest. This corresponds to the knee of the LC filter. For this system it is around 800 kHz. For frequency of interest, active damping leg is comparable to passive damping leg. Passive damping leg has lower impedance above and below frequency of interest.

below the corner frequency is inconsequential to its overall performance. The only thing that matters is its performance at the frequency of the knee of the LC filter. Experimental results show similar performance over this region. Therefore the active damping leg is comparable to a passive damping leg implemented with a 0.22 Ω resistor and a 1 μF capacitor.

E. Sensor Design

Both feedback and feedforward signals are sensed using high-pass filters feeding directly in to the gain amplifiers as illustrated in Fig. 5. This implementation proves to be efficient and straightforward for sensing ac signals, while rejecting the dc component. The pole of each filter is placed well below the fundamental ripple frequency to reduce magnitude and phase errors. Placing the pole a factor of 100 below the fundamental switching frequency gives about 0.6 deg of phase shift at the fundamental. The prototype has the poles about a factor of 700 below the fundamental switching frequency; the corresponding phase shift is only 0.07 deg.

III. EXPERIMENTAL RESULTS

The proposed hybrid passive/active filter technique has been applied to the design of an output filter for a 230 W buck converter operating at 14 V output from a 42 V nominal input (Fig. 11). The fundamental switching frequency is 125 kHz. The buck converter power stage utilizes a 1.4 μH inductor and 20 μF primary output capacitor and operates in discontinuous conduction mode under average current mode control.[2]

A structural view of the output filter and test setup is shown. The passive components of the hybrid filter comprises a 0.2 μF ceramic capacitor and a damping leg made up of a 1 μF electrolytic capacitor and a 0.22 Ω resistor. As described previously, this passive damping leg can be replaced with an active circuit and a significantly smaller capacitor (not shown in Fig. 11). Tests of the system were conducted using conventional EMI test procedures. A line impedance stabilization network (LISN) was placed between the load and the output filter. The LISN passes power frequency signals to the load, while acting as a known impedance at ripple frequencies. The voltage across the 50 ohm LISN resistor is used as the metric for output ripple performance. Tests described here were performed using a 1 Ω load.

The performance of the hybrid filter is determined by first taking measurements without injection from the active filter element. Essentially, the 5 μH magnetizing inductance of the injector transformer and the 0.2 μF output capacitor forms a conventional LC low-pass filter. Measurements were then taken with the active filter in operation. Fig. 12 illustrates the dramatic improvement in output voltage ripple performance that is achieved through the use of the active circuitry. The spectral measurements of Fig. 13 indicate that the use of active injection provides almost 35 dB reduction in fundamental ripple voltage and results in the largest component across frequency being 25 dB lower in magnitude.

As mentioned previously, the best results are achieved with feedforward and feedback control used together, as illustrated in Fig. 14. Individually, the feedforward and feedback controls above are able to

[2]The filter was designed to provide improved EMI performance for an existing power stage. While better results might be obtained by cooptimizing the power stage and filter, the results presented here reflect what is achieved with a single filter stage using passive and hybrid/active techniques for a specified noise source. We expect similar results in higher order filters and more highly optimized systems.

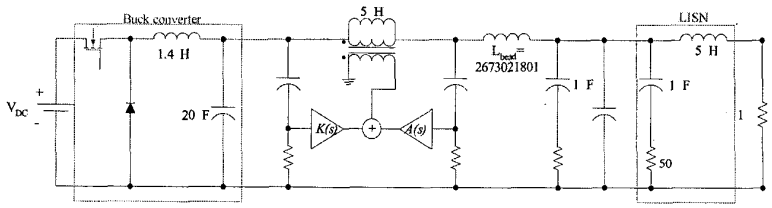

Fig. 11. Test setup for hybrid filter. Active filter used in conjunction with small passive output filter. Output filter consists of 0.2 μF capacitor in parallel with damping leg comprising a 0.22 Ω resistor and a 1 μF electrolytic capacitor.

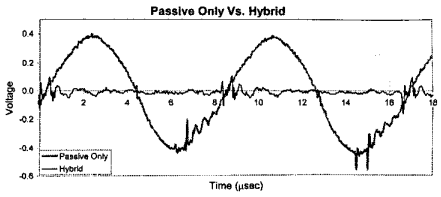

Fig. 12. Experimental test results for 125 kHz buck converter. Voltage ripple measured at LISN shown both with and without active injection. Peak-to-peak ripple greatly reduced by active circuit.

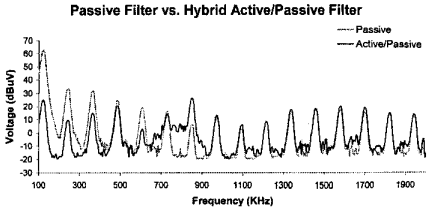

Fig. 13. Ripple spectra measured at output of LISN for both hybrid active/passive filter and passive filter of same size. Hybrid filter achieves a 35 dBμV attenuation of fundamental ripple frequency as compared with passive components alone.

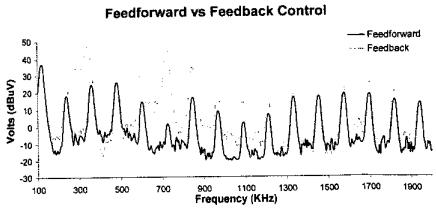

Fig. 14. Ripple spectra measured at output of LISN for feedforward and feedback control used individually. Measurement with active filter off offered for comparison. Each control technique has its own performance limitations. Feedback control actually performs worse than no active filtering at certain frequencies.

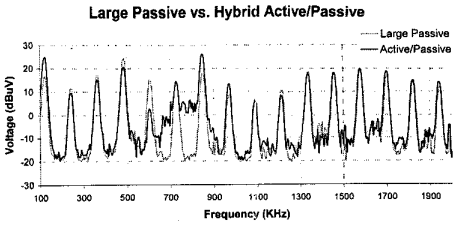

Fig. 15. LISN voltage spectra of hybrid active/passive filter and large passive filter with a 20 μF capacitor. Plots indicate that both hybrid filter and large passive filter both meet a flat 25 dBμV ripple specification across frequency.

achieve about 20 dB ripple attenuation, corresponding to about 10% residual ripple. The amount of attenuation attainable for feedforward is limited by phase and magnitude error. The feedforward control has very slight magnitude and phase errors, but they significantly limit feedforward ripple cancellation. For the feedback control, stability considerations limit achievable feedback gain and ripple attenuation. The ripple around 700 kHz is greater with feedback ripple cancellation than without, reflecting deterioration in filter performance in this region due to ripple *amplification* by the feedback. The increase in ripple from feedback control in the region is compensated by the feedforward control. Therefore, as illustrated in Fig. 13, the combination of the two control systems yields a superior result over either one alone. At mid-range frequencies the feedforward controller compensates for the limitations of the feedback controller, and at still higher frequencies only passive filtering is effective. These two complementary control schemes allow for the maximum usage of the injector.

In order to compare the benefits of hybrid filters with conventional passive filter design methods, a passive filter meeting the same ripple specification is designed using the 5 μH magnetizing inductance of the injector. The larger passive filter requires a 20 μF capacitor to meet the same flat ripple specification across frequency (ripple $\leq$ 25 dBμV across frequency). Relative performance of the hybrid filter and the large passive filter is shown in Fig. 15. Therefore, the hybrid filter allows a 20 μF capacitor to be replaced with a 0.2 μF capacitor with no degradation in performance. This corresponds to a factor of 100 reduction in the required filter capacitance utilizing the hybrid active/passive approach presented here. Furthermore, Fig. 10 shows that the active damping circuitry presented in Section II D provides identical performance to the purely passive damping leg. Therefore the active damping circuit provides a reduction in damping capacitance by a factor of 1000. Essentially, a simple, single transistor circuit is capable of making a 1 nF capacitor behave like a 1 μF capacitor. The benefit of the proposed approach is that by introducing simple, signal-level active circuitry, one can dramatically reduce the passive filter capacitance for the same level of performance.

The transient response of the power converter (e.g. during load steps) is another important performance metric. Fig. 16 shows experimental measurements comparing transient performance of the power converter with an active filter versus one with a passive filter. The passive filter is the same as the one above, a 5 μH inductor with a 20 μF capacitor. Fig. 16(a) shows load steps between 100% and 50% of full load, while Fig. 16(b) shows load steps between 100% and 25% of full load. The overall transient performance of the hybrid and passive filters are similar. It is of interest to note that the passive filter displays less damping in the step response as compared with the hybrid/active filter. This characteristic is attributed to the damping leg. Although both the hybrid and passive filters use the same damping leg, it was design specifically for the active filter. The above results demonstrate that

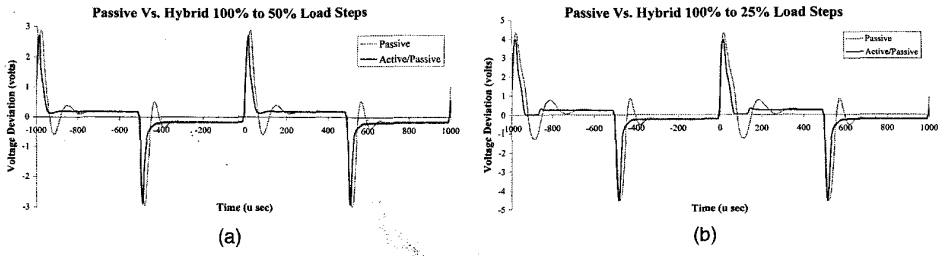

Fig. 16. (a) Transient response of load steps from full load to half load. (b) The transient response of load steps from full load to a quarter load. Both (a) and (b) show voltage deviation from 14 V dc versus time. Overall transient responses of power converter with active and hybrid filters are similar. Passive filter response slightly worse due to poor damping.

a hybrid filter can replace a passive filter with out eroding the transient performance.

The efficiency of the active filter is of great concern because it is dissipative in nature, unlike conventional passive filters. If the losses in the active circuitry greatly decrease the efficiency of the converter then the approach will not be worthwhile. In the prototype system, the active circuitry is powered from two small switching regulators connected to the buck capacitor (or the "noisy" 14 V side). The regulators take the noisy 14 V and supply a nearly steady $+/-6$ V. In many applications, separate generation of the signal-level voltages is not necessary. It is included here for completeness. Experimental results show that the average current is slightly less than 100 mA. This corresponds to 1.4 W of power dissipation. If the active damping is also used, then the power dissipation increases to 2 W. This corresponds to only 0.9% of the total output power. Thus, the active circuitry does not dramatically affect the efficiency of the overall system.

The proposed approach enables the replacement of a large-valued capacitor with a small valued capacitor plus an amplifier and an additional magnetic winding. This may or may not result in physical size reduction in the circuit (depending on specific component types), but is particularly advantageous if it is desirable to avoid electrolytic-type capacitors (e.g. for temperature or reliability reasons). In its present implementation the approach is unlikely to be advantageous in terms of cost due to the use of high-performance operational amplifiers as part of the active circuit.

IV. CONCLUSION

Active ripple filters can effect substantial reductions in power converter input and output ripple components, allowing considerable reduction in passive component size. This paper investigates a hybrid passive/active filter topology that achieves ripple reduction by injecting a compensating voltage ripple across a series filter element. Both ripple feedforward and feedback are employed. The design of sensor, amplifier, and injector circuitry suitable for the application is investigated. Furthermore, this paper explores the use of active damping and its ability to reduce shunt damping capacitance size. The experimental results demonstrate the feasibility and high performance of the new approach, and illustrate its potential benefits. It is demonstrated that the proposed approach is most effective in cases where it is desirable to minimize the amount of capacitance in the filter. In these cases, a capacitance reduction of a factor of 100 or more is possible with active filtering and active damping, without impacting ripple performance.

REFERENCES

[1] Phelps, T. K., and Tate, W. S. (1979)
Optimizing passive input filter design.
In *Proceedings of Powercon 6*, May 1979, G1-1–G1-10.

[2] Zhu, M., Perreault, D. J., Caliskan, V., Neugebauer, T. C., Guttowski, S., and Kassakian, J. G. (1999)
Design and evaluation of an active ripple filter with Rogowski-coil current sensing.
IEEE PESC Record, **2** (1999), 874–880.

[3] Feng, S., Sander, W. A., and Wilson, T. (1970)
Small-capacitance nondissipative ripple filters for dc supplies.
IEEE Transactions on Magnetics, **6**, 1 (Mar. 1970), 137–142.

[4] Hamill, D. C. (1996)
An efficient active ripple filter for use in dc-dc conversion.
IEEE Transactions on Aerospace and Electronic Systems, **32**, 3 (July 1996), 1077–1084.

[5] Poon, N. K., Liu, J. C. P., Tse, C. K., and Pong, M. H. (2000)
Techniques for input ripple current cancellation: classification and implementation.
IEEE Transactions on Power Electronics, **15**, 6 (Nov. 2000), 1144–1152.

[6] Walker, J. (1984)
Designing practical and effective active EMI filters.
In *Proceedings of Powercon 11*, 1984, I-3, 1–8.

[7] LaWhite, L. E., and Schlecht, M. F. (1987)
Active filters for 1 mHz power circuits with strict input/output ripple requirements.
IEEE Transactions on Power Electronics, **PE-2**, 4 (Oct. 1987), 282–290.

[8] Farkas, T., and Schlecht, M. F. (1994)
Viability of active EMI filters for utility applications.
IEEE Transactions on Power Electronics, **9**, 3 (May 1994), 328–337.

[9] Moon, M. S., and Cho, B. H. (1996)
Novel active ripple filter for the solar array shunt switching unit.
Journal of Propulsion and Power, **12**, 1 (Jan.–Feb. 1996), 78–82.

[10] Midya, P., and Krein, P. T. (1994)
Feed-forward active filter for output ripple cancellation.
Int. J. Elec., **77**, 5 (1994), 805–818.

[11] Casey, L. R., Goldberg, A., and Schlecht, M. F. (1988)
Issues regarding the capacitance of 1–10 mHz transformers.
In *Proceedings IEEE APEC*, 1988, 352–359.

[12] Goldberg, A., Kassakian, J. G., and Schlecht, M. F. (1989)
Issues related to 1–10 mHz transformer design.
IEEE Transactions on Power Electronics, **4**, 1 (Jan. 1989), 113–123.

[13] Vlatkovic, V., Borojevic, D., and Lee, F. C. (1996)
Input filter design of power factor correction circuits.
IEEE Transactions on Power Electronics, **11**, 1 (Jan. 1996), 199–205.

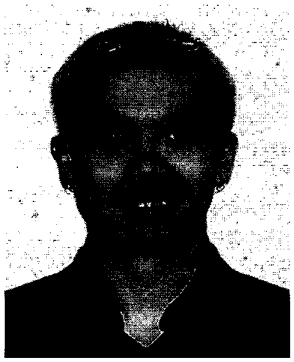

Albert C. Chow received the B.S. degree in electrical engineering from Columbia University, New York, NY, in 1999, and the S.M. degree from the Massachusetts Institute of Technology, Cambridge, in 2002, where he is currently pursuing the Ph.D. degree.

At present, his research interests are in areas of analog and digital circuits with emphasis on analog-to-digital converters, operational amplifiers, and power electronic systems. His doctoral research is directed toward the design of high speed analog-to-digital converters. Between 1999 and 2002, he worked on the reduction of passive components on power systems.

David J. Perreault (M'98) received the B.S. degree from Boston University, Boston, MA, in 1989, and the S.M. and Ph.D. degrees from the Massachusetts Institute of Technology, Cambridge, in 1991 and 1997, respectively.

In 1997 he joined the MIT Laboratory for Electromagnetic and Electronic Systems as a Postdoctoral Associate, and became a research scientist in the laboratory in 1999. In July of 2001, he joined the MIT Department of Electrical Engineering and Computer Science as an assistant professor. He teaches a graduate-level course in power electronics and is a consultant to industry in the field. At present, his research interests are in design, manufacturing, and control techniques for power electronic systems and components, and in their use in industrial, commercial, transportation, and medical applications.

Dr. Perreault is a member of Tau Beta Pi and Sigma Xi, and is a recipient of the IEEE Richard M. Bass Outstanding Young Power Electronics Engineer Award and the ONR Young Investigator Award.